Vegetation mapping using discrete-return and full-waveform airborne LiDAR data

Chen Dong[a,b], Zhang Liqiang[b,*], Xu Xiang[b], Wang Zhen[b]

[a]Nanjing Forestry University
[b]State Key Laboratory of Remote Sensing Science
Beijing Normal University
Beijing, China
chendong@njfu.edu.cn

Abstract—Vegetation mapping is a significant issue in city modeling and estimating vegetation properties. This paper aims to accurately extract vegetation point clouds from urban and mountainous areas using discrete-return and full-waveform airborne Light Detection and Ranging (LiDAR) data. For the full-waveform LiDAR data, the full-waveform decomposition and modeling technique based on kernel function is proposed to generate dense 3D point clouds. Then, the pre-segmentation algorithm based on probability density analysis is employed to generate homogenous segments for a supervised, segment-based SVM classifier, which uses more relevant features derived from geometric, radiometric, multi-echo and full-waveform attributes. Finally, Our approach is experimentally validated on the datasets from the Helsinki University of Technology, Finland and Dayekou, Zhangye City, Gansu Province, China.

I. INTRODUCTION

To acquire the accurate 3D point clouds for vegetation mapping, in this paper, the object-based vegetation extraction method is proposed using airborne LiDAR data from discrete-return TopEye sensor and full-waveform RIEGL LMS-Q560 scanner. We address the following objects. (*i*) Decomposition and modeling of waveform profiles by extensible kernel library using optimization technique; (*ii*) A pre-segmentation by the probability density clustering for the subsequent segment-based SVM classifier; (*iii*) Extraction of relevant features from both full-waveform backscattered amplitude profiles and discrete point clouds for segment features calculation and (*iv*) Hierarchical object-based classification framework to extract vegetation point clouds using these relevant segment features.

II. MATERIALS

A. Study areas

Two airborne LiDAR datasets of Helsinki (Fig. 1a) and Dayekou (Fig. 1b) were used to evaluate the robustness of the proposed approach.

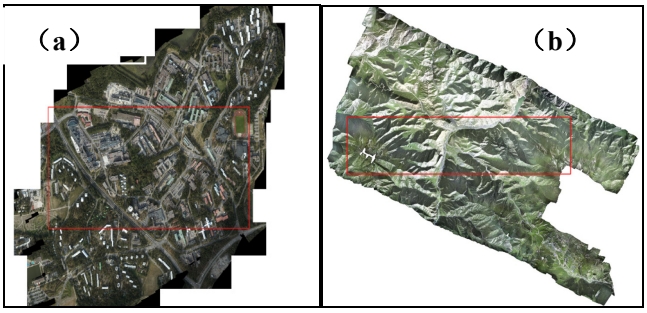

Fig1. Aerial image of the study area in (a) Helsinki and (b) Dayekou

B. Data sets

The discrete-return TopEye instrument system was used to conduct the Laser campaigns of Helsinki University of Technology in September 2002. It can only simultaneously acquire the first and last pulse point clouds and the helicopter-borne TopEye system (wavelength of 1064 nm, maximum scan angle ±20°) was used to collect laser data at flying altitudes of 200 m and 550 m.

For the other study area of Dayekou, the full-waveform data with the coordinate system of the UTM/WGS 84 at the zone of 32 was used in this paper. It were captured by Y-12 airplane, which carried the LiteMapper 5600 full-waveform airborne LiDAR system at 1GHz frequently sampling rate in June 2008. The LiteMapper system adopted in this paper used a RIEGL LMS-Q560 laser scanner with near-infrared (1550 nm) laser pulses and a transmitted pulse width of 4 ns. It has a laser beam divergence angle of 0.5 mrd, which produces a footprint diameter of approximately 0.38 m on the target at nadir. The laser scanning pulse rate was 50 KHz and the maximum scan angle for data set was ±22.5° from nadir.

III. METHODOLOGY

A. Full-waveform decomposition and modeling techniques

(1) Savitzky-Golay filtering

As shown in Fig. 2, the raw backscattered profile includes actual signal and noise. To uncover the regular pattern and provide the reliable signal for calculating robust initial parameters in full-waveform decomposition and modeling process, the Savitzky-Golay (SG) smoothing filter (Savitzky *et al*., 1964) is selected to smooth the equally time spaced full-waveform signals.

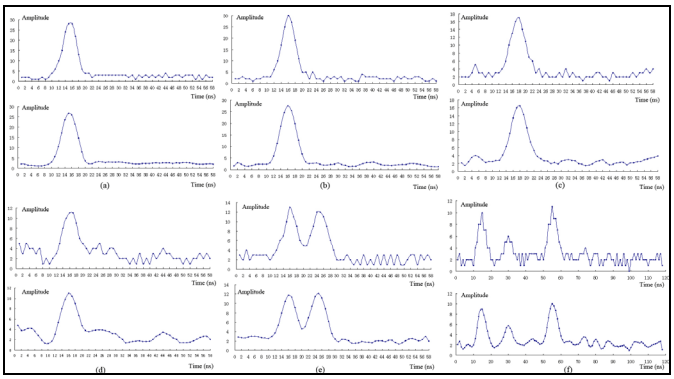

Fig. 2 Savitzky-Golay (SG) smoothing for some typical full-waveform backscattering pulses.

(2) Full-waveform decomposition and modeling

The waveform airborne backscatter signal is composed of points uniformly spaced $(x_i,y_i)_{\{i=1,\ldots,N\}}$ sampled at 1 GHz for our Riegl LMS-Q560 point clouds, and the energy function is described as:

$$\theta^* = \arg\min_{\theta} \frac{1}{N-p}\sum_{i=1}^{N}(y_i - \sum_{j=1}^{n} P_j(x_i,\theta) - \varepsilon) \qquad (1)$$

where N is the number of samples; n is the number of components, representing the targets located within the travel path; p is the number of parameters of the fitting functions, and $P_j(x_i,\theta)$ represents the given kernel function. Three kernel functions are used in this paper: (*i*) the Gaussian and general Gaussian kernels are used to process symmetrical backscattered echoes; (*ii*) the Nakagami kernels are employed to process left-skewed or right-skewed echoes.

Since the composition of kernels is varied, the traditional Gaussian-Newton or Levenberg-Marquardt algorithm cannot solve the above non-convex energy function. To deal with this problem, the reversible jump Markov chain Monte Carlo (MCMC) sampler (Hastings, 1970) coupled with simulated annealing are used to find the global minimum. As shown in Fig. 3, The typical full-waveform backscattering pulses are modeled by the above proposed method.

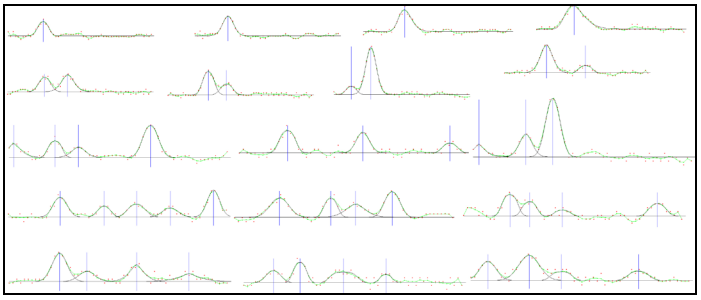

Fig. 3 Results of typical full-waveform fitting on Dayekou airborne LiDAR pulses. The red points denote the raw digitalized backscatter signals; The green and black profiles indicate the smoothed signals and the modeled backscattered signals, respectively.

(3) Generation of three-dimensional point clouds

When the optimal location of each backscattered echo T_j is obtained, the corresponding discrete point clouds X_j are analyzed by:

$$X_j = X_{start} + C(T_j - T_{start})d_{start}(j = 1,\ldots,n) \qquad (2)$$

where X_{start}, d_{start} and T_{start} are the first sample of start pulse waveform, the emitted laser pulse direction, and the start

time of the waveform, respectively; n is the number of detected targets or components per emitter laser pulse; C is the speed of light.

B. Pre-segmentation

Object-based classification approach has already proven to be a high suitability for pixel classification. In this section, the pre-segmentation method (Poullis *et al.*, 2009) based on probability density clustering is proposed to segment discrete point clouds, and the pre-segmentation results are prepared for the subsequent segment-based SVM classifier. The pre-segmentation result is shown in Fig. 4.

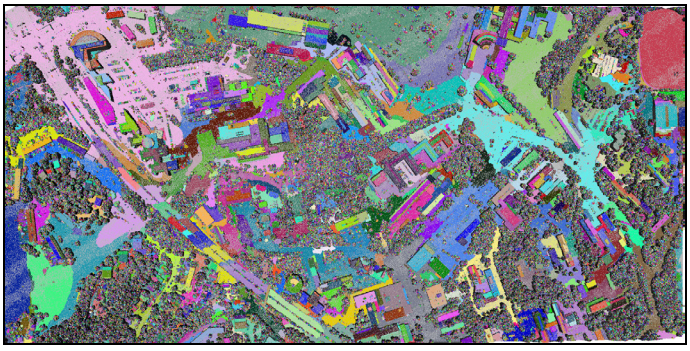

Fig. 4. Pre-segmentation results based on probability density clustering. Note that the colors are reused and may appear in different regions.

C. Extraction attributes from full-waveform profiles

Through the Eq. (1), the optimal T_j, A_j and σ_j of each backscatter echo j are obtained. The parameter A_j should be corrected to eliminate the fluctuation effects of the emitted power E, the incidence angle α and the range R. The corrected procedure is described as:

$$A_j^{'} = \frac{A_j}{\alpha}\frac{A_{mean}}{A_{current}}\frac{R^2}{R_s^2} \tag{3}$$

where A_{mean} is the average amplitude value of all emitted pulses and $A_{current}$ is the amplitude of the emitted pulse of the current peak. R, R_s and α are the range between the current target and the sensor, a standard range for the whole survey area and the incident angle between the laser beam and the estimated local plane, respectively. The full width at half maximum (FWHM) echo W_j can be inferred by:

$$W_j = 2\sqrt{2\ln 2}\sigma_j \tag{4}$$

Based on the radar equation, the "apparent" cross-section σ^j of each detected backscatter echo j derived by Wagner *et al.* (2006), which is defined as:

$$\sigma^j = C_{cal} R^4 A_j \sigma_j \tag{5}$$

where C_{cal} is the calibration constant, which is calculated by the process of Lehner and Briese (2010) where a portable reflectometer and spectralon targets are used to estimate calibration constant of in situ radiometric reference targets (*e.g.*, asphalt areas close to nadir view for each LiDAR strips). R is the range from the sensor to the target.

Furthermore, σ^0 is the cross-section normalized by the illuminated area s_j [m^2 m^{-2}], which is described as:

$$\sigma^0 = \frac{\sigma^j}{s_j} \tag{6}$$

The used of σ^0 has advantages that measures of radar system with different spatial resolution can be easily compared, when σ^j increases in general with s_j. However, when α is changed, the corresponding illuminated area s_j is also changed, so the cross-section σ^j is also related to the incoming beam. The backscatter coefficient γ is the cross-section normalized by the incoming beam and described as:

$$\gamma = \frac{4\sigma^j}{\pi R^2 \beta^2} \tag{7}$$

When the reflected target is an area-extend targets, *i.e.*, the size is larger than the footprint size of the sensor, the γ is also equal to Eq. (8), which can be considered as σ^0 corrected by incidence angle α.

$$\gamma = \frac{\sigma^j}{s_j \cos\alpha} \tag{8}$$

The four full-waveform attributes (*i.e.*, echo width W, backscatter cross-section σ, backscatter cross-section per illuminated area σ^0 and backscatter coefficient γ) derived from the full-waveform airborne LiDAR data are referred to as radiometric information.

D. Extraction features from discrete point clouds

In this section, the radiometric, Height-based, Plane-based,

Eigenvalue-based and multi-echo features are extracted form discrate airborne LiDAR point clouds. For more details of feature definition, please refer to the related paper (Mallet *et al*., 2011).

IV. CLASSIFICATION

In this section, non-parametric method, *i.e.*, SVM classifier is employed to classify the segments. It performs a robust non-linear classification of samples using the diversity kernel functions with a small number of parameters, and can effectively avoid over-fitting and under-fitting problems during learning from samples. As shown in Figs. 5 and 6, the accurate vegetation points are extracted from Finland and Dayekou data sets.

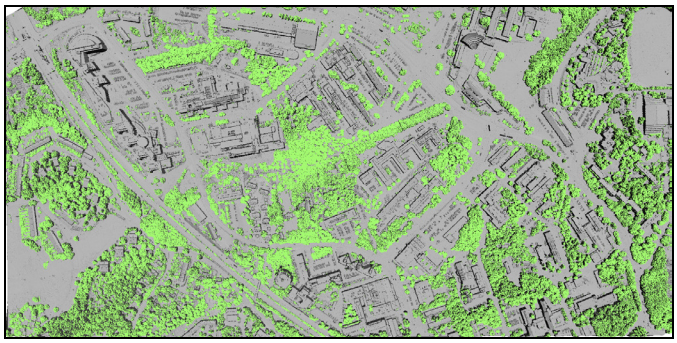

Fig. 5. The classification results of the Helsinki dataset.

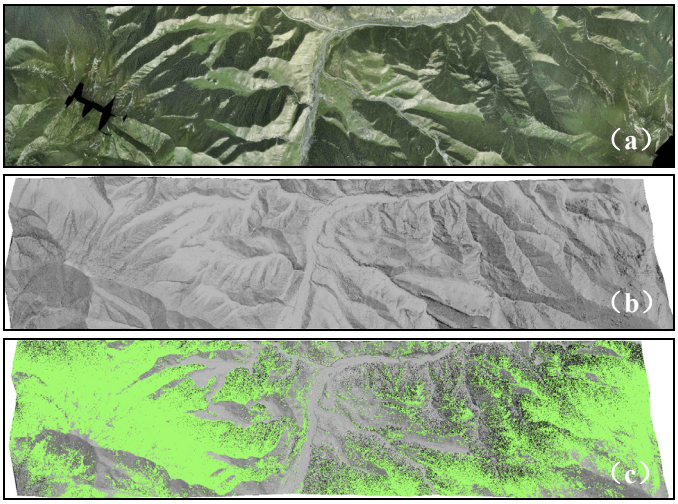

Fig. 6. The classification results of the Dayekou dataset. (a) The multispectral ortho-image. (b) The generated DEM. (c) The extracted vegetation points (light green color) are overlaid on their digital surface model.

V. CONCLUSION

The segment-based classification algorithm exhibits more significant features and robust classification than point-wise or pixel-wise classification. The combination of full-waveform attributes and geometrical featues derived from discrete point clouds can sigmificantly improve the accurate vegetation mapping. In our further research, the full-waveform, LiDAR data will be employed to acquire more plentiful information that is based on a radiation mechanism. Additionally, for high density point clouds, vegetation structure models will be integrated into our future work for better vegetation extraction.

ACKNOWLEDGEMENT

We are grateful to the editors and reviewers for their valuable comments and suggestions which have helped us improve the context and presentation of the paper. The study is supported by National Natural Science Foundation of China (No. 41301521).

REFERENCES

[1] Savitzky, A., Golay, M.J.E., 1964. Smoothing and differentiation of data by simplified least squares procedures. Analytical chemistry, 36(8):1627-1639.

[2] Hastings, W. K., 1970. Monte Carlo sampling methods using Markov chains and their applications, Biometrika, 57(1):97-109.

[3] Poullis, Charalambos You, Suya, 2009. Automatic reconstruction of cities from remote sensor data. IEEE Conference on Computer Vision and Pattern Recognition, 2775-2782.

[4] Wagner, W., Ullrich, A., Ducic, V., Melzer, T., Studnicka, N., 2006. Gaussian decomposition and calibration of a novel small-footprint full-waveform digitising airborne laser scanner. ISPRS Journal of Photogrammetry and Remote Sensing, 60(2):100-112.

[5] Lehner., H., Brese, C., 2010. Radiometric calibration of full-waveform airbrone laser scanning data based on natural surfaces. International Archives of Photogrammetry Remote Sensing and Spatial Information Sciences. XXXVIII, part7B, 360-365.

[6] Mallet, C., Bretar, F., Roux, M., Soergel, U., Heipke, C., 2011. Relevance assessment of full-waveform lidar data for urban area classification. ISPRS Journal of Photogrammetry and Remote Sensing, 66(6): 71-84.